Fusion Engineering and Design 202 (2024) 114308

Contents lists available at ScienceDirect

Fusion Engineering and Design

journal homepage: www.elsevier.com/locate/fusengdes

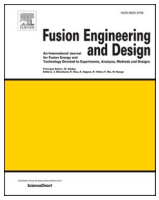

Design status of the neutron and gamma-ray diagnostics for the Divertor Tokamak Test facility

D. Marocco [a,*], M. Angelone [a,d], F. Belli [a], F. Caruggi [b], G. Croci [b], B. Esposito [a], G. Gandolfo [a], G. Gorini [b], G. Grosso [c], M. Nocente [b], F. Panza [a], M. Pillon [a], F. Pompili [a], D. Rigamonti [c], G. Rocchi [a], J. Scionti [c], M. Tardocchi [c]

[a] Fusion and Technology for Nuclear Safety and Security Department, ENEA C.R. Frascati, Frascati 00044, Italy
[b] Department of Physics, University of Milano-Bicocca, 20126 Milan Italy
[c] Institute for Plasma Science and Technology, National Research Council, Milan 20125, Italy
[d] Industrial Engineering Department, University of Rome "Tor Vergata", Roma 00100, Italy

ARTICLE INFO

Keywords:
Divertor tokamak test (DTT) facility
Neutron and gamma-ray detectors
Runaway electrons
fast ions

ABSTRACT

In the frame of the design activities of the Divertor Tokamak Test (DTT) facility the development of a comprehensive set of neutron and gamma-ray diagnostics is on-going in order to enable measurements of: neutron yield, neutron yield rate, neutron emissivity over a poloidal section through the plasma; neutron emission spectrum; runaway electrons induced bremsstrahlung radiation and gamma-ray emission from reactions between fast ions and plasma impurities. The present paper provides an overview of the DTT neutron and gamma-ray diagnostics and describes the present status of their design including main components and interfaces, detector types and performances.

1. Introduction

The Divertor Tokamak Test Facility (DTT) is a fully superconducting nuclear fusion device under design and construction in Italy, with the main aim of developing alternative solutions to the heat exhaust in DEMO [1]. During the first phase of plasma operations (phase 1, 2029), 4 MW of ICRH and 16 MW of ECRH will be available at the site. The installation of 10 MW of NNBI and additional 4 MW of ICRH and 16 MW of ECRH will be completed during the second DTT operational phase (phase 2, 2032). DTT will work with deuterium fuel; the yield rate of 2.45 MeV neutrons is expected to vary in the range 3.6×10^{14}–1.5×10^{17} n/s and the emission of 14.1 MeV neutrons due to triton burn-up (TBN) will be up to few per cent of 2.45 MeV neutrons [2].

Neutron diagnostics are key DTT systems since the measurement of the neutron emission (time-integrated, space/time-resolved) will provide an indication of the performance of the facility in the different magnetic field configurations (e.g. single null, double null, snowflake) and divertor solutions (e.g. liquid metals) planned for the operation. Moreover, they can provide a measurement of Runaway Electrons (REs), which represent a major threat in the operation of tokamaks; REs are electrons that, having gained an energy greater than a critical value, are continuously accelerated by the toroidal electric field and may damage in-vessel components when losing confinement. The interaction of REs with plasma ions and tokamak components produces bremsstrahlung radiation that can be measured by using detectors sensitive to hard x-rays [3].

Both neutron and gamma-ray diagnostics will provide insights on the dynamics of fast ions by measuring, respectively, the non-thermal components of the neutron emission spectrum [4] and the gamma-rays emitted in nuclear reaction between the ions and plasma impurities [5].

In order to cover the measurements of the quantities mentioned above a joint work between ENEA, CNR and University of Milano-Bicocca is on-going for the design and manufacturing of the following diagnostics: neutron activation system (NAS); time-resolved neutron yield monitors (NYM); neutron and gamma-ray camera (NGC); time of flight spectrometer (TOF); the location of the diagnostics in DTT is sketched in Fig. 1. The NAS and the NYM are Phase 1 diagnostics that will be present since the day-zero of DTT operations, while NGC and TOF will be operational for phase 2. An overall description of the DTT neutron and gamma-ray diagnostics is provided in the following sections of the paper, together with a summary of the design activities performed

* Corresponding author.
E-mail address: daniele.marocco@enea.it (D. Marocco).

https://doi.org/10.1016/j.fusengdes.2024.114308
Received 13 October 2023; Received in revised form 29 February 2024; Accepted 1 March 2024
Available online 12 March 2024

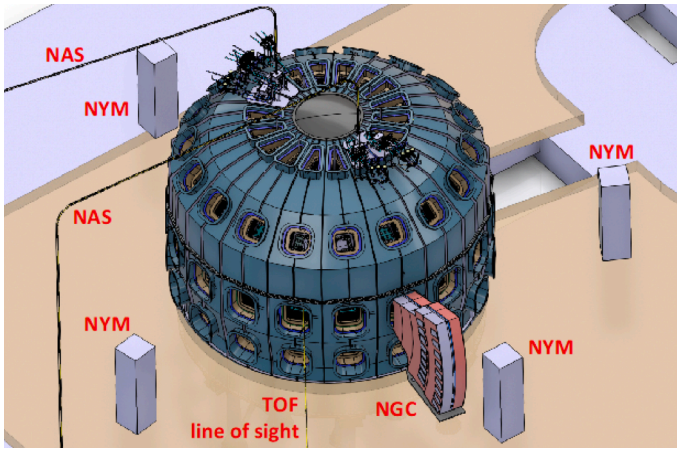

Fig. 1. Location of neutron and gamma-ray diagnostics in DTT.

so far.

2. DTT neutron and gamma-ray diagnostics

2.1. Neutron activation system (NAS)

The NAS is a diagnostic dedicated to the measurement of the neutron Yield (total number of neutrons emitted in a DTT pulse). The Yield measurements are based on the detection of the gamma-rays emitted by activated foils hosted in aluminium capsules and moved, by means of a pneumatic system, between a dedicated laboratory located outside the Torus Hall and a measurement position located close to the plasma boundary. The gamma-ray measurements, performed after removing the foils from the capsule in order to avoid measuring the background signal due to the activation of the capsule itself, will allow to determine the neutron fluence at the measurement position; the yield is then derived through the application of calibration factors determined by MCNP calculations and in-situ measurements performed with neutron sources (^{252}Cf, DD and DT neutron generators) [6]. Being in close proximity to the plasma NAS remains unaffected by modifications in the tokamak hall and can be also used to monitor/cross-calibrate the NYM.

NAS measurement positions are foreseen in two DTT vertical ports (sector #1 and sector #11). Each port hosts a stainless steel pipe called irradiation end (diameter=28 mm, length= 4 m) at the end of which the aluminium capsule is positioned during plasma pulses (Fig. 2).

The irradiation end will be connected, outside the vacuum boundary, to three flexible plastic pipes ~ 37 m long running up to the NAS laboratory: a main pipe dedicated to the transport of the activation samples (28 mm diameter) and two pipes for pressurized air (21 mm diameter).

The NAS laboratory will host a send/return station for each of the irradiation ends. The station, managed by a dedicated PLC, is composed by a photo detector and a pressure switch monitoring the presence of the capsule (respectively in the NAS laboratory and in the irradiation end) and a set of six solenoid valves managing the airflow during send/return operations. The laboratory will also host a high purity germanium (HPGe) detection system for gamma-ray counting. The system includes an HPGe detector (60 % relative efficiency) with associated cooling system, lead shield and acquisition chain.

Indium (for 2.5 MeV neutrons), aluminum and niobium (for 14.1 MeV TBN neutrons) are presently considered as activation foil materials (see Table 1). The use of additional foils enabling spectrum unfolding can be envisaged especially in the calibration phase in order to improve the reliability of the NAS MCNP model.

In order to characterize the radiation field at the level of the irradiation end and to have a preliminary indication of the foil thickness needed during operations a dedicated MCNP analysis was carried out. The irradiation end including the aluminium capsule and the activation foil positioned at the measurement location have been integrated into the DTT 20° model [2]; first wall cooling pipes were also included in the model since potentially affecting the results. Neutron spectra and fluxes were calculated using both DD and DT neutron sources and were then scaled by the neutron yields calculated for low-power, half-power and full-power scenarios described in [7] (Table 2 and Fig. 3 (top)).

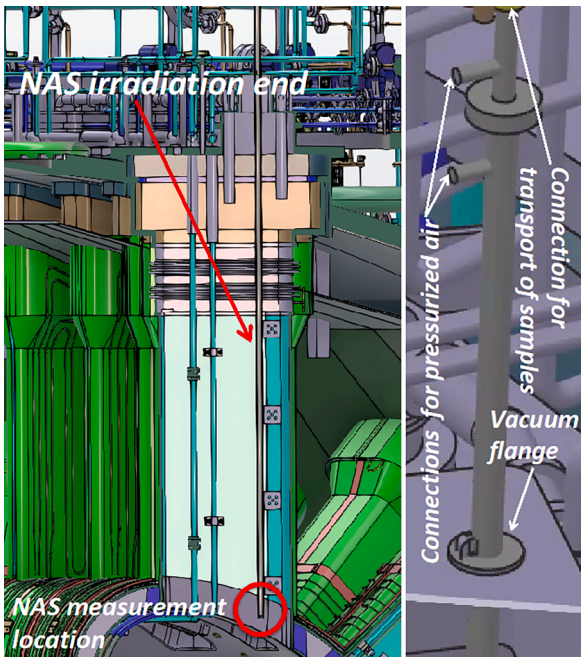

Fig. 2. Layout of a NAS irradiation end in the port (left). Detail of the irradiation end connections (right).

Table 1
Candidate activation materials for DTT NAS.

Element	Reaction of interest	Threshold (MeV)	Half Life	Gamma-ray energy (keV)
In	^{115}In(n,n')^{115}In^{m}	0.6	4.486 h	336.24
Al	^{27}Al(n,p)^{27}Mg	4.3	9.6 min.	843.8/
	^{27}Al(n,α)^{24}Na	6.8	15 h	1014.44 1368.63
Nb	^{93}Nb (n,2n)^{92}Nb^{m}	9	10.25 days	934.5

The MCNP spectra were used to evaluate, through FISPACT-II 5.0, the induced activity (A_0) for different foil thicknesses and materials. Calculations were performed considering an irradiation time equal to the expected duration of a DTT pulse (100 s) and a cooling time varying with the selected material in order to ensure the decay of other interfering radionuclides (4 h for indium, 0.5 h for aluminum and 3 h for niobium).

Finally, the counts in the region of interest (ROI) detected by the HpGe detector for a fixed acquisition time t_m and the limit for quantitative analysis (L_Q, number of net recorded counts above which a

Table 2
Yield rates of plasma scenarios used for NAS simulations.

Scenario	DD Yield rate (s^{-1})	TBN fraction (%)	DT Yield rate (s^{-1})
Low-power [1]	2.3×10^{14}	2.8	6.4×10^{12}
Half-power [2]	2.3×10^{16}	4.4	9.8×10^{14}
Full-power [3]	1.3×10^{17}	5	6.5×10^{15}

[1] Scenario A1 in [7]: 8 MW ECRH.
[2] Scenario C1 in [7]: 16 MW ECRH + 4 MW ICRH.
[3] Scenario E1 in [7]: 32 MW ECRH + 8 MW ICRH + 10 MW NNBI.

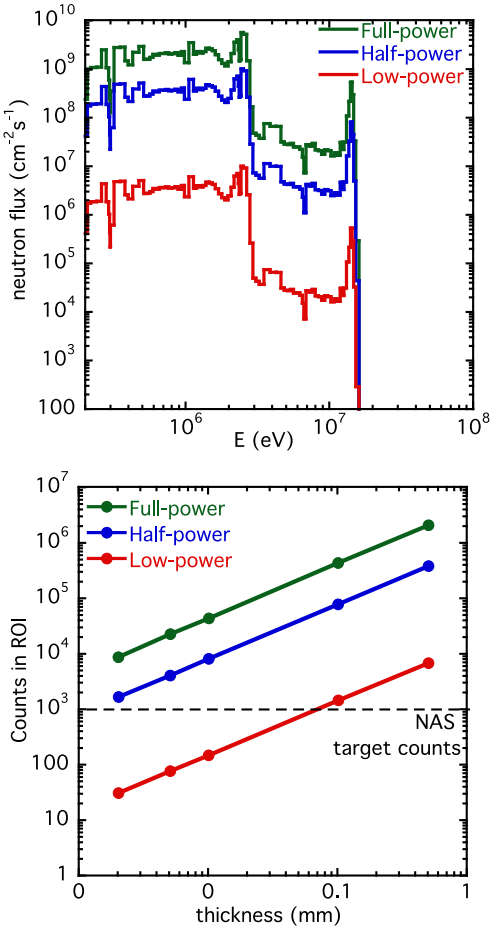

Fig. 3. DD and DT neutron spectra at the NAS measurement position for different DTT scenarios (top). HPGe counts in the region of interest vs. thickness of indium foils for different DTT scenarios (bottom).

quantitative analysis of the gamma spectrum in the ROI is possible, [8]) were estimated using the formula below:

$$counts\ in\ ROI = \frac{A_0(1-e^{-\lambda t_m})}{\lambda}\frac{\varepsilon\ P_\gamma}{K_\mu};$$

$$L_Q = 50\left\{1+\left[1+\frac{R_{bkg}t_m}{12.5}\right]^{1/2}\right\}$$

where A_0 is the activity after the cooling time, λ is the decay constant of the analyzed radionuclide, ε is the detector measurement efficiency, P_γ is the gamma ray emission probability, K_μ is a corrective coefficient taking into account the attenuation of gamma-rays due to the activation foil material itself and R_{bkg} is the background count rate. A target of at least 1000 counts in the ROI (3 % statistical error) was selected and the acquisition time was set to 3600 s since for such value the limit for quantitative analysis resulted much smaller than 1000 counts for all the considered nuclides.

Fig. 3 (bottom) shows the results of the analysis in the case of indium and indicates that the minimum foil thickness enabling to cover all DTT operational scenarios within requirements is ~ 0.1 mm. The same analysis carried out for aluminum and niobium indicates that foils with thicknesses ~ 1 mm are adequate for operations above half power, while for day-zero operations the recorded counts are significantly less than 1000 even assuming 5 mm thick foils, and thus suggests that in these cases the acquisition time should be increased or the foils moved closer to the detector.

2.2. Neutron yield monitors (NYM)

The NYM are active detectors distributed in the torus hall around the machine, dedicated to the measurement of the neutron yield rate (Y). The detectors provide count rate measurements that are converted into yield rate through the application of calibration factors that, as in the case of NAS, are obtained through MCNP calculations and in-situ calibration [6].

The present strategy for the implementation of the DTT NYM is that of adapting the set of detectors formerly used at the Frascati Tokamak Upgrade (FTU), which consists of:

- Sixteen ^{235}U Fission chambers (FCs) working in count mode (4 sets of 4 detectors with fixed ^{235}U coating mass: 4×10^{-2} g; 4×10^{-3} g; 4×10^{-4} g to 4×10^{-5} g). The FCs are embedded in moderator-shielding units composed by a mixture of lead (80 % in weight) and polyethylene.
- Three couples of BF3 proportional counters working in count mode. Each couple is composed by a low sensitivity detector (embedded in a moderator-shielding unit composed by a mixture of polyethylene and boron) and a high sensitivity detector (without moderator-shielding unit).
- One 5 × 5 inch NE213 liquid scintillator working in current mode.
- One 3 × 3 inch NaI scintillator working in count mode.

Four provisional installation locations have been identified between equatorial ports of DTT sectors #1 and #2, #4 and #5, #10 and #11 and #15 and #16.

BF3s and FCs have low sensitivity to hard x/gamma-rays[1] and, once calibrated, provide a measurement of the neutron yield rate. NE213 and NaI scintillators are instead sensitive both to neutrons and to hard x/gamma-rays. In RE free discharges they provide a measurement that is proportional to the yield rate and they can be cross-calibrated with BF3s/FCs, while in presence of REs they measure an excess signal due to the RE-induced bremsstrahlung radiation. The difference between the calibrated signals of NE213/NaI and BF3/FCs can be used to provide an indication of RE intensity [3].

A preliminary analysis was carried out to assess the performances of BF3s and FCs in DTT. MCNP calculations of the neutron flux as a function of the distance from DTT axis were performed using the DTT 360° model [2], in order to take into account the scattering contribution of the torus hall walls. The scoring positions were chosen on the DTT mid-plane between two equatorial ports. The fluxes were combined with the flux efficiency of the detectors (counts per unit flux) in order to determine the detectors' count rates at the different positions; Fig. 4 shows the estimated count rates at full power in the case of FCs.

The calculated count rates were used to check the performance of the detectors considering the following requirements/assumptions:

- Maximum statistical error with which the count rate (CR) should be measured $\Delta CR/CR \leq 3$ %.
- Time resolution (i.e. time within which a measurement complying with previous requirement should be provided) $\Delta t \leq 100$ ms.
- Maximum count rate sustainable by detectors $CR_{max}\sim1\times10^6$ cps (counts per second).

Fig. 5 (top) shows, as an example, the behaviour of the statistical error as a function of the time resolution in the case of a 10^{-2} g ^{235}U FC. Calculations are performed with the FC located at the two extreme positions in the torus hall (cryostat and at torus hall walls) and for different yield rate values. Results indicate that, independently from the position,

[1] FCs can detect foto fission events due to gammas with energy above ~7 MeV produced by thick-target bremsstrahlung of REs with tokamak structures during disruption events.

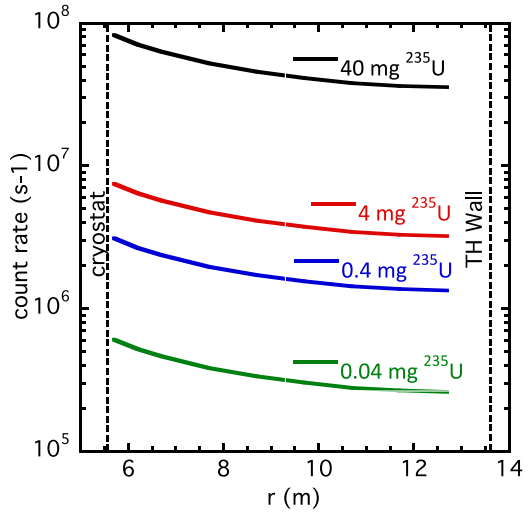

Fig. 4. FC count rates vs. distance from DTT axis (full power).

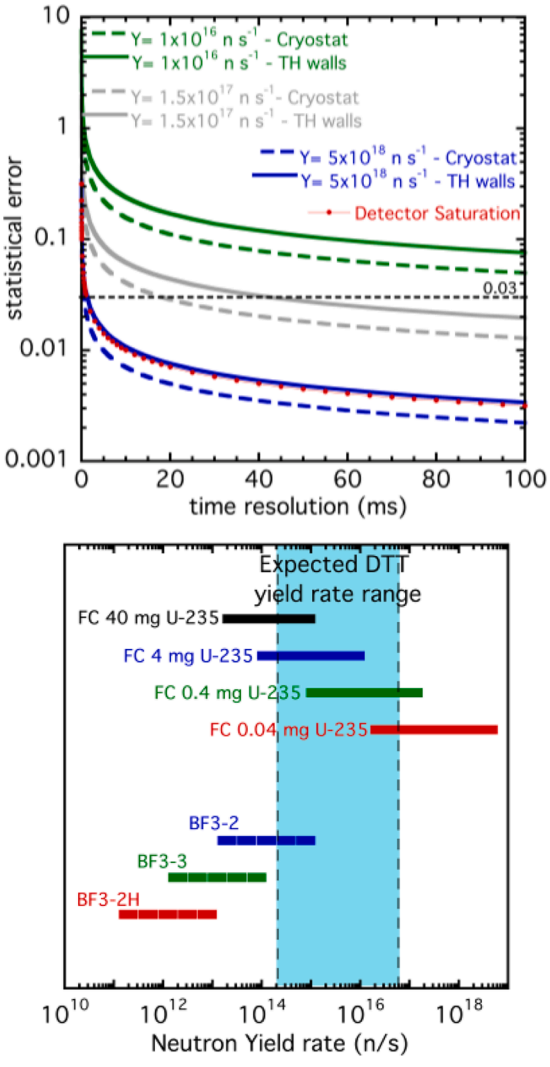

Fig. 5. Statistical error vs. time resolution at different neutron yield rates for a 0.04 mg ^{235}U FC located close to cryostat or to Torus Hall (TH) walls (top). FCs and BF3s coverage of DTT neutron yield rate range (bottom).

the detector starts meeting the time resolution requirement (3 % statistical error in 100 ms) for yield rates higher than Y~10^{16} n/s and that the detector's count rate is below 1 × 10^6 cps up to Y~ 5 × 10^{18} n/s.

The results of the overall analysis are summarized in Fig. 5 (bottom) and indicate that the FCs can cover the full range of the yield rates expected in DTT within requirements and with a good degree of overlapping between the operating range of the different detectors; the FCs also allow operation within requirements above 1.5 × 10^{17} n/s and below 3.6 × 10^{14} n/s. BF3s overlap with FCs in the lower part of DTT yield rate range (1 × 10^{14} n/s - 1 × 10^{15} n/s) and can extend the NM operating range down to Y~1 × 10^{11} n/s, thus improving the capability to monitor the ramp-up and ramp down phases of DTT pulses.

2.3. Neutron and gamma ray camera (NGC)

The NGC is a diagnostic devoted to spatially resolved measurements of the neutron emission, the RE-induced bremsstrahlung radiation and the gamma-ray emission from reactions between fast ions and plasma impurities. Volume integration of the neutron emissivity profile provided by the NGC can also be used to derive an independent estimate of the neutron yield rate to be compared with NYM measurements; conversely, the neutron yield rate provided by NYM can be used as a constraint in the neutron emissivity reconstruction algorithm used by the NGC.

The diagnostic is composed by a massive shielding block located in the torus hall in front of the equatorial port of DTT sector #1 (Fig. 6). The shielding block features a central unit composed by two stainless steel slabs in which a fan shaped collimating structure is machined (9 lines of sight (LOS), length= 2 m, diameter= 2 cm); the aperture of the fan is defined in order to maximize plasma coverage. Neutron detector boxes are located at the end of the collimators; neutron attenuators and gamma-ray detector boxes are located behind neutron detectors. The stainless steel slabs are surrounded by the actual shielding material, which is further enclosed in a stainless steel shell; candidate shielding materials are concrete and an hydrogenated borate mix proposed for the ITER radial neutron camera (JC277-5, [9]).

Based on FTU/JET experience and on ITER design activities, several candidate detectors have been identified for the neutron camera unit: plastic scintillators (EJ-276 G, [10]), liquid scintillators (EJ301, [11, 12]), ^{4}He scintillators [13], single Crystal Diamonds (sCD) [14]. ^{4}He gas scintillator represents a promising alternative to liquid and plastic scintillators since shows a linear relationship between the incident neutron energy and the maximum light output, is potentially insensitive to radiation damage and does not present fire hazards. Scintillator containing chlorine (CLYC, $LaCl_3$:(Ce)) are also being investigated; these are inorganic scintillators whose interaction with the 2.5 MeV neutrons generates, through nuclear reactions, a characteristic peaked response in the neutron energy spectrum [15]. The practical consequence is a better separation between the direct and the scattered neutron components and enhanced neutron spectroscopy capabilities; measurements at the Frascati Neutron Generator [16] are on going in order to characterize the properties of such detectors.

Based on JET experience Lanthanum Bromide scintillators doped with Cerium ($LaBr_3$:Ce) and Lithium hydride (LiH) capsules have been chosen as gamma camera detectors and attenuators, respectively [17]. A length of ~ 63 cm has been selected for the attenuator based on MCNP calculations (Fig. 7). For such length the ratio between the attenuation factors for 2.45 MeV neutrons and 4.44 MeV gamma-rays[2] is ~800, which is deemed sufficient to ensure measurements with an acceptable signal-to-background ratio.

MCNP calculations using point detector tally (F5) were also carried out to evaluate the fluxes and spectra of uncollided and collided

[2] Energy of gamma-rays from ^{3}He+^{9}Be or alpha+^{9}Be reactions, which have been measured in many experiments at JET; other lines of interest are typically in the range up to 5 MeV.

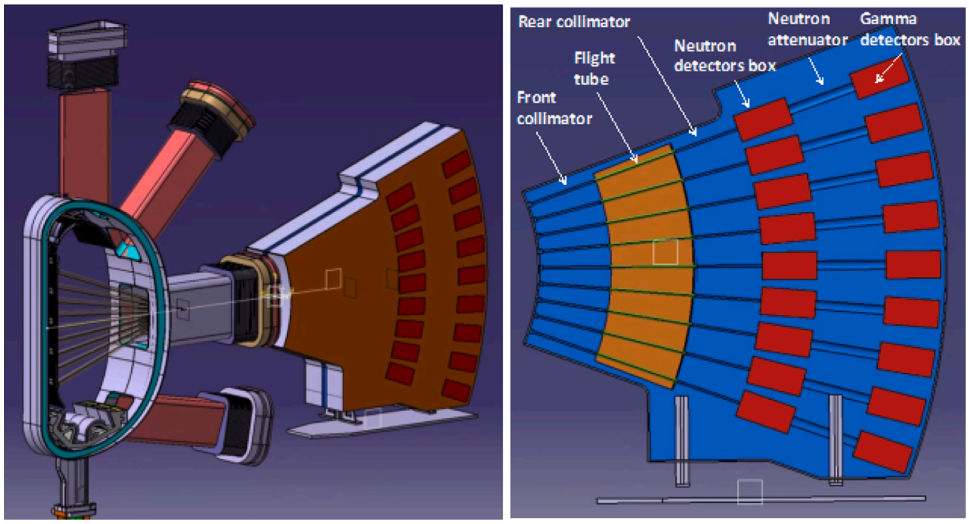

Fig. 6. DTT neutron/gamma camera layout (left). Detail of one of the two slabs of the collimating unit (right).

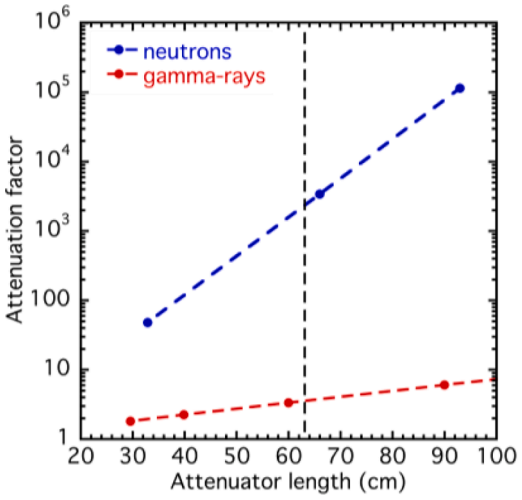

Fig. 7. Attenuation factors of LiH for 2.45 MeV neutrons and 4.44 MeV gamma-rays vs. LiH thickness.

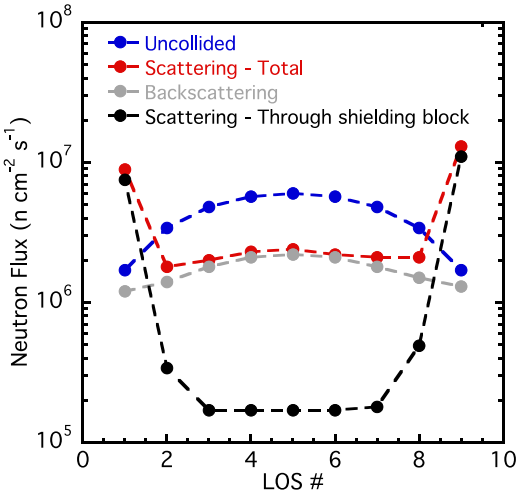

Fig. 8. Neutron flux components at NCG neutron detector positions (full power).

(scattered) neutrons at the neutron detector positions. A dedicated analysis was performed in order to decouple the scattered neutrons reaching the detectors after having crossed the shielding block (scattering through shielding block) from those reaching the detectors travelling along the collimators after having scattered in the vessel region opposite to each LOS (backscattering). The first component can be reduced by modifying the layout and/or the material of the block, while the second depends on the vessel material/geometry and on the he position of the LOS and can't be suppressed by improving the shielding design. Results of the calculations for full power operations (Fig. 8), carried out by filling the collimators with a neutron absorber and by suppressing all neutrons having at least one interaction in the shielding block, indicate that, except for edge channels, the background is always between 40 % and 60 % of the signal due to uncollided neutrons and is composed almost entirely by backscattered neutrons. In the edge LOS (#1 and #9) the scattering is between 5 and 7 times higher than the signal and is largely due to scattering through the shielding block, indicating that the shielding in this region needs to be optimized. The layout of the camera has been updated and new calculations are on going to check the performance of the new layout. It should be anyway mentioned that the analysis presented above represent a first approximation, since the actual signal to background ratio depends on the specific detector and can be estimated by folding the collided and uncollided components of the neutron spectrum with the detector response function and setting a proper energy threshold.

Performance calculations were carried out in order to define a reference subset of NGC detectors (^{4}He, plastic/liquid scintillators and sCD).

The same requirements and assumptions considered for the NYM were used (see Section 2.2) and reference flux values at different DTT yield rates were defined by scaling the full power flux of a central NGC LOS (#5). The efficiencies of the detectors were then identified by varying design parameters such as the thickness (liquid/plastic scintillators and sCD) and the pressure (^{4}He) in order to have a detector set covering the DTT yield rate range with: at least 1 detector matching requirements; overlap of the operating range of at least two detectors. The output of the analysis is summarized in Fig. 9 and the set of candidate detectors is shown in Table 3. The 2 inches plastic/liquid scintillator will cover low to mid neutron yield rates (Y~10^{14} - 10^{16} n/s) and the 50 bar ^{4}He mid to high yield rates; the other two detectors will provide redundancy by overlapping with the ^{4}He and the 2 inches scintillator. Above the working limit of the ^{4}He the diagnostic will saturate, while below the working limit of the 2 inches scintillator the time resolution of the diagnostic will be higher than 100 ms.

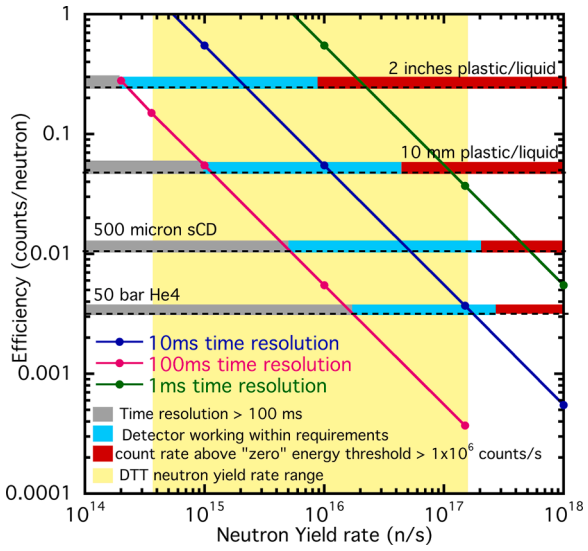

Fig. 9. Performance of a subset of NGC detectors.

Table 3
Candidate subset of NGC neutron detectors.

Detector	Design parameter	Energy threshold (MeV)	ε_0* (counts /neutron)	ε_M** (counts/ neutron)
^{4}He	50 bar pressure	1.6 neutron energy	1.6×10^{-2}	3.1×10^{-3}
Pl./liq. scintillator	1 cm thickness	1.6 neutron energy	1.1×10^{-1}	4.8×10^{-2}
Pl./liq. scintillator	2 inch thickness	1.6 neutron energy	5.7×10^{-1}	2.4×10^{-1}
sCD	500 μm thickness	0.3 deposited energy	2.4×10^{-2}	1.0×10^{-2}

* Efficiency above a "zero" energy threshold higher than the electronic noise level, to be considered for maximum count rate calculations.
** Efficiency above the energy threshold set for DD measurements.

2.4. Time of flight spectrometer (TOF)

The TOF is a neutron diagnostic dedicated to the high-resolution measurement of the neutron emission spectrum along a collimated LOS. Joint analysis of TOF outputs and those provided by the NGC neutron and gamma-ray detectors will provide a detailed description of the different components of the neutron emission spectrum and of the underlying ion populations.

In its original layout, the TOFOR diagnostic implemented at JET [18], the neutron beam impinges on a scintillator (S1), which scatters the neutrons that are then detected by a set of secondary scintillators (S2) (Fig. 10, left). S1 and S2 detectors sit on the sphere of constant time of flight and the energy of the neutron impinging on S1 is given by

$$E_n = 2m_n\left(\frac{r}{t_{TOF}}\right)^2$$

where m_n is the neutron mass, r the radius of the sphere and t_{TOF} the measured time of flight of the scattered neutron. In the TOFOR-II design, implemented by the TOFED diagnostics at EAST [19], each of the S2 scintillators is divided in two segments. Moreover, digital data acquisition is used to measure the energy of the scattered neutrons in order to discriminate those that originate from a true scattering event in S1 from the accidental background, such as that due to gamma-rays and multiple neutron scattering in the instrument. The result is a significant suppression of the intrinsic background of the instrument in the region that corresponds to neutron emission from supra-thermal ions.

An update of the TOFED design (TOF-X) is proposed for DTT, with the inclusion of an additional set of forward detectors placed at a low scattering angle in order to enable measurements of the 14 MeV neutrons. Moreover, a gamma-ray spectrometer (same detector and attenuator of the gamma camera unit, Section 2.3) is included in the TOF-X design in order to combine neutron and gamma-ray spectroscopy techniques along the same LOS and to enable RE measurements (Fig. 10, right). The diagnostic will be located outside the torus hall and dedicated penetrations are foreseen in the buildings to allow the TOF LOS to look at the plasma through the equatorial DTT port in sector #17.

TOF-X will have the same energy resolution and flux efficiency for 2.5 MeV neutrons of the TOFOR/TOFED (7–8 % and 0.12 cm^{-2} respectively) since the geometry that is used to detect 2.5 MeV neutrons in TOF-X is unchanged; preliminary analyses suggest similar performances also for the measurement of 14 MeV neutrons. For full power operations the maximum count rate on S2 detectors is expected to be ~ 5

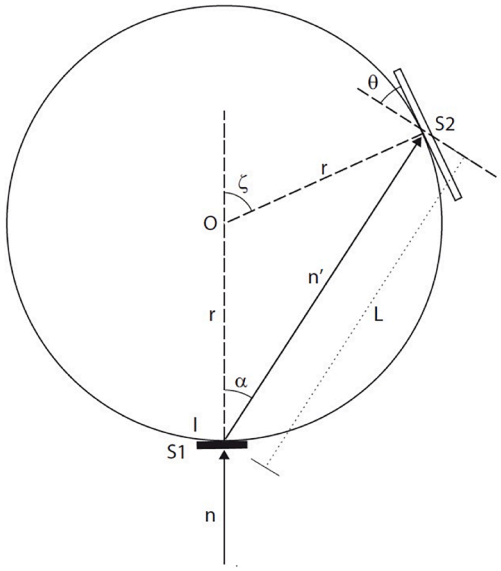

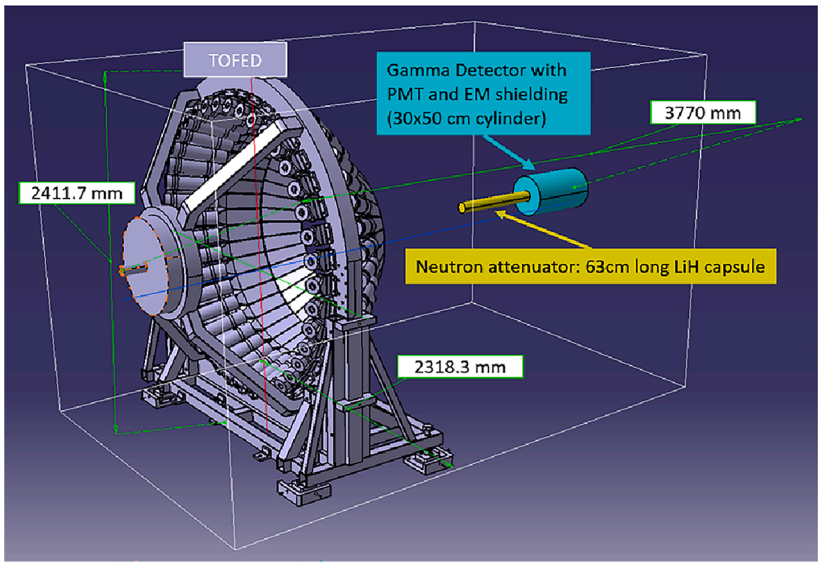

Fig. 10. Sketch of TOFOR concept (left). DTT TOF layout (right).

$\times 10^5$ cps for 2.5 MeV neutrons [20] and, assuming a value of 7 % for the TBN fraction in the core, $\sim 3.5 \times 10^4$ cps for 14 MeV neutrons. The figure for 2.5 MeV neutrons is close to the limit of the instrument but still of no concern for the collection of high quality data. The development of a full Monte Carlo model of the detector with the GEANT4 code is presently on going in order to verify the results of such preliminary analysis and to provide a detailed response function of the instrument.

3. Conclusions

The paper presented the whole set of DTT neutron and gamma-ray diagnostics. The neutron activation system will measure the DTT neutron yield using indium, aluminum and niobium activated foils. The overall NAS design is defined, including the pneumatic system handling the foils and the gamma-ray detection system. The next step of analysis will be dedicated to the definition of the calibration procedure.

The neutron yield monitors will measure the neutron yield rate and the intensity of REs by adapting the detectors formerly used in the Frascati Tokamak Upgrade (fission chambers, BF3 proportional counters, NE213 and NaI scintillators). Results of the design activities indicate that the available detectors are suited to cover the DTT neutron yield rate range. Definition of the calibration procedure will now be addressed together with that of NAS.

The neutron and gamma-ray camera will measure the profiles of the emitted neutrons, the gamma-rays due to reactions between fast ions and plasma impurities and the hard x-rays due to REs bremsstrahlung. A preliminary design of the diagnostic in terms of LOS geometry and materials of the shielding block and the collimators (concrete/borated hydrogenated mix and stainless steel, respectively) has been defined. Candidate neutron detectors have been identified and a preliminary selection has been made (50 bar ^{4}He scintillator, 1 cm and 2 inches plastic/liquid scintillator, 500 μm thick sCD). Gamma–ray detectors and associated neutron attenuators have been identified (lanthanum bromide scintillators doped with cerium and lithium hydride, respectively).

The TOF will provide a high-resolution measurement of the spectrum of 2.5 MeV and 14 MeV neutrons along a LOS; gamma-ray measurements will be enabled by the inclusion of a dedicated spectrometer along the same LOS. The conceptual design of the diagnostic has been proposed and semi-analytical estimates of the diagnostic flux efficiency (0.12 cm^{-2}), energy resolution (7 - 8 %) and maximum expected count rate ($\sim 5 \times 10^5$Ccps) have been provided. Definition of the detailed response function of the detector through Monte Carlo simulations is presently on going.

CRediT authorship contribution statement

D. Marocco: Conceptualization, Formal analysis, Project administration, Validation, Visualization, Writing – original draft, Writing – review & editing. **M. Angelone:** Conceptualization, Writing – review & editing. **F. Belli:** Formal analysis. **F. Caruggi:** Methodology, Visualization. **G. Croci:** Formal analysis. **B. Esposito:** Conceptualization. **G. Gandolfo:** Formal analysis, Methodology, Software, Writing – review & editing. **G. Gorini:** Conceptualization. **G. Grosso:** Formal analysis. **M. Nocente:** Conceptualization, Formal analysis, Writing – review & editing. **F. Panza:** Formal analysis, Methodology, Software, Writing – review & editing. **M. Pillon:** Conceptualization. **F. Pompili:** Formal analysis. **D. Rigamonti:** Conceptualization, Formal analysis, Writing – review & editing. **G. Rocchi:** Methodology, Visualization. **J. Scionti:** Formal analysis, Methodology, Software. **M. Tardocchi:** Conceptualization, Formal analysis.

Declaration of competing interest

The authors declare that they have no known competing financial interests or personal relationships that could have appeared to influence the work reported in this paper.

Data availability

Data will be made available on request.

References

[1] R. Ambrosino, DTT-divertor tokamak test facility: a testbed for DEMO, Fus. Eng. Des. 167 (2021) 112330.
[2] R. Villari, Nuclear design of divertor tokamak test (DTT) facility, Fus. Eng. Des. 155 (2020) 111551.
[3] B. Esposito, Runaway electron generation and control, Plasma Phys. Control. Fusion 59 (2017) 014044.
[4] J. Eriksson, Measuring fast ions in fusion plasmas with neutron diagnostics at JET, Plasma Phys, Control. Fusion 61 (2019) 014027.
[5] M. Nocente, MeV range particle physics studies in tokamak plasmas using gamma-ray spectroscopy, Plasma Phys. Control. Fusion 62 (2020) 014015.
[6] D.B. Syme, Fusion yield measurements on JET and their calibration, Fus. Eng. Des. 89 (2014) 2766–2775.
[7] I. Casiraghi, Core integrated simulations for the divertor tokamak test facility scenarios towards consistent core-pedestal-SOL modeling, Plasma Phys. Control. Fusion 65 (2023) 035017.
[8] L.A. Currie, Limits for qualitative detection and quantitative determination Application to Radiochemistry, Anal. Chem. 40-3 (1968) 586–593.
[9] https://johncaunt.com.
[10] B. Esposito, Progress of design and development for the ITER radial neutron camera, J. Fusion Energy 41 (2022) 22.
[11] J.M. Adams, The JET neutron emission profile monitor, NIM-A 329 (1993) 277–290.
[12] D. Marocco, First results on runaway electron studies using the FTU neutron camera, Fus. Eng. Des. 96–97 (2015) 852–855.
[13] Q. Ducasse, Characterization of the response and the intrinsic efficiency of a ^{4}He scintillation detector to fast mono-energetic neutrons, NIM-A 998 (2021) 165168.
[14] M. Passeri, Neutron/Gamma separation in 500μm thick single crystal diamonds, NIM-A 974 (2020) 164195.
[15] A. Giaz, The CLYC-6 and CLYC-7 response to g-rays, fast and thermal neutrons, NIM-A 810 (2016) 132.
[16] M. Martone, The 14 MeV Frascasti Neutron Generator, Journal of Nuclear Matererial 212-215 (1994) 1661–1664.
[17] M. Nocente, A new tangential gamma-ray spectrometer for fast ion measurements in deuterium and deuterium–tritium plasmas of the Joint European Torus, Rev. Sci. Instrum. 92 (2021) 043537.
[18] M. Gatu Johnson, the 2.5-MeV neutron time-of-flight spectrometer TOFOR for experiments at JET, NIM-A 591 (2008) 417–430.
[19] Xing Zhang, Diagnosing NB plasmas on the EAST tokamak with new time-of-flight neutron spectrometer, Nuclear Fusion 54 (2014) 104008.
[20] M. Cecconello, Conceptual design of a collimated neutron flux monitor and spectrometer for DTT, Fus. Eng. Des. 167 (2021) 112382.